ACTA
AMAZONICA | http://dx.doi.org/10.1590/1809-4392202403143

MATERIALS TECHNOLOGY | ORIGINAL ARTICLE

Removal of Cr (VI) from synthetic effluents using hydrochar from waste açaí (*Euterpe precatoria* Mart.) seeds as a low-cost biosorbent

Railane Inácio Lira dos SANTOS[1,2*], Luís Fernando Lira SOUTO[2], Nathiely Andrade de MORAES[2], Ana Clara de Sousa MENDES[2] , Naelly Nayllén Alves ARAÚJO[2], Flávio Augusto de FREITAS[3]

[1] Universidade Federal do Amazonas, Programa de Pós-Graduação em Química - UFAM, Manaus – AM, 69080-900, Brazil

[2] Instituto Federal de Rondônia - IFRO, Porto Velho – RO, 76820-441, Brazil

[3] Centro de Bionegócios da Amazônia - CBA, Manaus – AM, 69075-351, Brazil

* Corresponding Autor: railane.santos@ifro.edu.br

ABSTRACT

Chromium (Cr) is a common contaminant in aquatic ecosystems, and in its hexavalent form (Cr (VI)) can cause serious risks to human health. This study utilized açaí waste to prepare a novel hydrochar (AWR) for Cr (VI) removal. AWR was characterized by Boehm titration, point of zero charge, infrared spectroscopy, thermogravimetric analysis, specific surface area measurement, scanning electron microscopy, and elemental analysis. A 2^3 factorial design examined the influence of key factors (pH, hydrochar mass, and Cr (VI) concentration). Results showed that acidic functional groups predominate on the surface of AWR. Under optimal conditions (pH = 2, hydrochar mass = 0.150 mg, and solution concentration = 150 mg L^{-1}), Cr (VI) removal exceeded 96% with maximum adsorption capacity (Q_{max}) = 20.60 mg g^{-1} at 35°C. Adsorption kinetics followed a pseudo-second-order model, and the Tenkin isotherm best described the data. Thermodynamic analysis indicated that Cr (VI) adsorption is spontaneous and endothermic. This study demonstrated that AWR is a novel, effective, and cost-effective adsorbent for removing Cr (VI) from water environments.

KEYWORDS: Residual biomass; heavy metals; absorbent; hydrothermal carbonization.

Remoção de Cr (VI) de efluentes sintéticos usando hidrocarvão de sementes residuais de açaí (*Euterpe precatoria* Mart.) como biossorvente de baixo custo

RESUMO

Cromo (Cr) é um contaminante comum em ecossistemas aquáticos, e na sua forma hexavalente (Cr (VI)) pode causar sérios riscos à saúde humana. Este estudo utilizou resíduos de açaí para preparar um novo hidrochar (AWR) para remoção de Cr (VI). O AWR foi caracterizado por titulação de Boehm, ponto de carga zero, espectroscopia de infravermelho, análise termogravimétrica, medição de área de superfície específica, microscopia eletrônica de varredura e análise elementar. Um planejamento fatorial 2^3 examinou a influência de fatores-chave (pH, massa de hidrochar e concentração de Cr (VI)). Os resultados mostraram que grupos funcionais ácidos predominam na superfície do AWR. Sob condições ótimas (pH = 2, massa de hidrochar = 0,150 mg e concentração da solução = 150 mg L^{-1}), a remoção de Cr (VI) excedeu 96% com capacidade máxima de adsorção (Qmax) = 20,60 mg g^{-1} a 35°C. A cinética de adsorção seguiu um modelo de pseudo-segunda ordem, e a isoterma de Tenkin descreveu melhor os dados. A análise termodinâmica indicou que a adsorção de Cr (VI) é espontânea e endotérmica. Este estudo demonstrou que o AWR é um adsorvente novo, eficaz e econômico para a remoção de Cr (VI) de ambientes aquosos.

PALAVRAS-CHAVE: Biomassa residual; metais pesados; adsorvente; carbonização hidrotérmica.

CITE AS: Santos, R.I.L.; Souto, L.F.L.; Moraes, N.A.; Mendes, A.C.S.; Araújo, N.N.A.; Freitas, F.A. 2025. Removal of Cr (VI) from synthetic effluents using hydrochar from waste açaí (*Euterpe precatoria* Mart.) seeds as a low-cost biosorbent. *Acta Amazonica* 55: e55mt24314.

INTRODUCTION

Industrial discharge of heavy metals, especially chromium (Cr), pollute water and threaten human health (Liu *et al*. 2024). This metal is discharged into water bodies through industrial activities such as mining, leather processing and finishing, refractory steel production, and electroplating (Zulfiqar *et al*. 2023). Hexavalent chromium (Cr (VI)) is highly toxic due to its solubility, mobility, and carcinogenicity (Nur-E-Alam *et al*. 2020; Koc *et al*. 2024). Bioaccumulation and chronic exposure to Cr (VI) cause several pathophysiological failures, including wounds, dermatitis, anemia, allergic reactions, and damage in the gastrointestinal tract and liver (Habib *et al*. 2024; Katsas *et al*. 2024). Therefore, developing efficient methods to remove Cr (VI) from the environment is urgent.

Removal of Cr (VI) includes precipitation (Yang *et al*. 2025), ion exchange (Tan *et al*. 2024), reverse osmosis (Nie *et al*. 2024), coagulation (Chen *et al*. 2024), and adsorption (Li *et al*. 2025). Of these, adsorption is the simplest, cheapest, and easiest to work with (Tee *et al*. 2022; Irshad *et al*. 2023). Ideal adsorbents combine large adsorption capacity, eco-friendliness, and sustainability (Tounsadi *et al*. 2025). Biomass-derived material, particularly agricultural waste, show promise as adsorbents for heavy metal removal (Rohman *et al*. 2024; Wibowo *et al*. 2024). One particularly useful way of using this biomass waste is to convert it into carbonaceous biosorbent material through thermochemical treatment (Bian *et al*. 2019, Maniscalco *et al*. 2020).

Hydrothermal carbonization (HTC) is a clean, low-energy method for biomass processing (Malool and Moraveji 2025). HTC operates at moderate temperatures (180 - 350°C) for 0.5h - 24h, under autogenous pressures (25 - 60 bar), using water as the reaction medium (Li *et al*. 2021; Țurcanu *et al*. 2022). During HTC, the biomass undergoes hydrolysis, dehydration, decarboxylation, polymerization, and aromatization, forming a solid product of hydrothermal carbon with the same energy level as bituminous coal, known as hydrochar (HC) (Fang *et al*. 2018, Dang *et al*. 2023).

Hydrochar provides economic and practical advantages, including no dehydration needs, higher yield, many functional groups, and a moderate pH (Guo *et al*. 2024). In addition, hydrochar is obtained at a relatively lower temperature compared to pyrolysis, resulting in lower energy consumption (Elhassan *et al*. 2024). Applications span energy production, soil amendment, and environmental remediation (Magdziarz *et al*. 2020, Thakur 2024). Biomass-derived hydrochar stands out for its low environmental impact and stability at low pH (Zhen *et al*. 2025). Hydrothermal carbonization also valorizes biomass waste into value-added products (Arevalo-Gallegos *et al*. 2017; de Freitas *et al*. 2024). Each kind of feedstock yields a hydrochar with distinct properties (e.g., functional groups, porosity, adsorption capacity) that influence their effectiveness in heavy metal removal (Zhang and Zhang 2022, Li *et al*. 2025).

Açaí fruits are derived from two palm species, *Euterpe oleracea* Mart. and *Euterpe precatoria* Mart. (de Freitas *et al*. 2024), They are known for their high energy and nutritional value (Melo *et al*. 2021). Pulping generates seed waste is often inappropriately discarded (Sato *et al*. 2019). Hydrochar from açaí waste is rarely reported and serves as a zero-cost carbon precursor. Its synthesis reduces costly sorbent expenses, reduces greenhouse gas (GHG) emissions, ensures carbon capture, offers a low-carbon economy, and enhances sustainability (Yadav *et al*. 2025).

This study used açaí waste to prepare novel hydrochar for Cr (VI) removal. Factorial design to test its effectiveness was applied to minimize time and costs. Hydrochar biosorption performance and cost assessment highlight açaí biomass valorization for toxic heavy metals removal and circular bioeconomy promotion.

MATERIALS AND METHODS

Hydrochar production

In Manaus, Amazonas, Brazil, açai seeds were collected, washed, dried (60°C), crushed, sieved (~ 2 mm), and dried again (103°C, 24 h). The product was mixed with distillate water (1:10 m/v ratio) in a 100 mL hydrothermal reactor and heated at 220°C for 6 h. The solid product was vacuum filtered, washed to neutral pH, dried (105°C overnight), and designated "hidrodrocarvão de Açaí" or Açaí Water Reactor (AWR).

Chemicals

A stock solution of potassium dichromate ($K_2Cr_2O_7$, 1 mol L^{-1}) was prepared in distilled water and adjusted to the desired pH. Working solutions with target Cr (VI) concentrations were obtained by appropriate dilution with double-distilled water. Hexavalent chromium (Cr (VI)) concentrations were determined using UV–Vis spectrophotometry at 540 nm with 1,5-diphenylcarbazide in acidic medium, according to ABNT (1996). For surface functional group analysis of the açaí seed-derived hydrochar, NaCl (≥ 98%), $NaHCO_3$ (≥ 99.7%), and Na_2CO_3 (≥ 99.0%) were used. Solution pH was adjusted using NaOH (98%) and HCl (37%). All reagents were of analytical grade and supplied by Merck.

AWR hydrochar characterization

Boehm titration (direct method) quantified the functional groups of hydrochar. The equilibrium batch method in triplicate determined the point of zero charge (pH_{PCZ}). The pHpcz was obtained from the initial pH vs. final graph. FTIR (Shimadzu spectrophotometer, IRAffinity-1) technique analyzed hydrochar functional groups. Thermogravimetry techniques (TG/DTG) tested the thermal stability of the hydrochars (SHIMADZU thermal analyzer, model TGA-51, under an N_2 atmosphere). Hydrochar morphology was observed via scanning electron microscope (SEM; TESCAN

VEGA 3). Surface area was measured using a Micromeritics (TriStar II 3020 V1.03). The sample chemical elemental analysis (C, H, and N) was conducted in a PE 2400 Series II CHNS/O analyzer. The Oxygen content was determined by subtracting the CHN results from 100%.

Biosorption tests - Factorial experimental design

A 2^3 factorial experimental design was carried out in duplicate, totaling 16 randomly performed tests. Analyzed variables were pH, hydrochar mass (*m*), and Cr (VI) concentration (*Conc*). The response variable was the percentage of Cr (VI) removal, using real and coded values (Table 1). Main effects, interactions between variables, and linear model regression coefficients were analyzed using Student's t-test ($\alpha = 0.05$). Analysis of variance (ANOVA) tested the model ($\alpha = 0.05$). The coefficient of determination (R^2) and the F-test were used as analysis criteria ($\alpha = 0.05$). R software (version 4.3.1) was used to determine the set-up of factorial designs and statistical analysis.

In the factorial design experiments, adsorption tests were performed in 16 Erlenmeyer flasks under constant stirring for 24 h. After the contact period, the contents of the flasks were centrifuged, and the supernatant was collected to determine the residual Cr (VI) concentration. The analysis was performed by measuring the absorbance at 540 nm by the diphenylcarbazide colorimetric method (ABNT, 1996). The hydrochar adsorption capacity at equilibrium (Qe, mg/g) and the percentage of Cr (VI) removal (R%) were determined using Equation 1 for capacity and Equation 2 for removal.

$$Q_e = (C_0 - C_e).\frac{V}{m} \quad (1)$$

$$R\% = \frac{(C_0 - C_t)}{C_0}.100 \quad (2)$$

where:

Q_e: Cr (VI) adsorbed per adsorbent mass of (g g^{-1}); Ci: initial Cr (VI) concentration (mg L^{-1}); Ce: equilibrium Cr (VI) concentration (mg L^{-1}); V: solution volume (L).

To study the adsorption kinetics of Cr (VI) on hydrochar, the material was placed in a shaker at 25°C, at the optimum dosage of the adsorbent, the pH and the optimum concentration of Cr (VI) obtained by the experimental design (150 mg L^{-1}, 0.150 mg AWR, at pH 2). Samples of the supernatant from the mixture (adsorbate/adsorbent) were evaluated in the range of 0 to 1440 min and then centrifuged for 20 min at 3000 rpm. Finally, the Cr (VI) concentration was measured by UV-visible spectrometry and applied pseudo-first order (PFO) and pseudo-second order (PSO) adsorption models (Eqs. S1–S2).

Isothermal experiments were conducted in duplicates using a 20 mL Cr (VI) solution concentration of 150 g L^{-1}, 150 mg AWR, at pH 2. The mixture was agitated in a shaker at a controlled temperatures (25, 35, and 45°C) for 60 minutes. Different isotherms were tested by Langmuir, Freundlich, and Temkin models (Eqs. S3, S4, S5).

Thermodynamic parameters are calculated by Gibbs free energy (ΔG°), enthalpy (ΔH°), and entropy (ΔS°) (Eqs. S6, S7, S8), and used to compare adsorption at different temperatures.

Table 1. Parameters and coded values used in the factorial experimental design.

Parameter	Level	
	-1	+1
pH	2.0	10.0
Hydrochar mass (mg)	0.050	0.150
Concentration of $K_2Cr_2O_7$ (mg/L)	50	150

RESULTS

AWR hydrochar characterization

The hydrochar derived from açaí seed waste (AWR) had acidic functional groups (0.072 mmol g^{-1}) dominated by carboxylic (0.045 mmol g^{-1}) and lactonic groups (0.022 mmol g^{-1}), with minimal phenolic groups (0.005 mmol g^{-1}), while basic groups measured 0.004 mmol g^{-1} (Table 2). Elemental analysis revealed a carbon content of 65.21%, hydrogen 6.60%, nitrogen 2.08%, and oxygen and other elements 26.11%, with ash content below 1% (Table 2). The surface area was 18.90 m^2 g (Table 2), and the pH at the point of zero charge of hydrochar was 4.94 (Figure 1A).

The FTIR spectrum of AWR revealed several characteristic absorption bands associated with specific functional groups. A broad band at ~3400 cm^{-1} was attributed to O–H stretching vibrations, indicating the presence of hydroxyl groups. Bands at 2928-2840 cm^{-1} are attributed to C–H stretching vibrations of aliphatic chains. The absorption band at 1700 cm^{-1} was attributed to C=O stretching of carbonyl groups, while the

Table 2. Contents of the elemental composition, atomic ratio, ash, surface area, and surface groups on the açaí seed hydrochar (AWR).

Elemental composition (%)	
N	2.08
C	65.21
H	6.60
O	26.08
Atomic ratio	
H/C	0.01
O/C	0.53
Ash (%)	0.025
Surface area (m^2 g^{-1})	18.90
Surface groups (mmol g^{-1})	
Carboxylic	0.045
Lactones	0.022
Phenolic	0.005
Total Acids	0.072
Total Basics	0.004

bands at 1610 cm^{-1}, 1510 cm^{-1}, and 1450 cm^{-1} were attributed to C=C stretching vibrations from aromatic structures. Additional bands at 1235 cm^{-1} and 1057 cm^{-1} are attributed to C–O stretching of ether/alcohol groups, and C–N stretching vibrations. The band at 756 cm^{-1} is attributed to the presence of aromatic C–H bending (Figure 1B).

Scanning electron microscopy (SEM) revealed irregularly shaped carbon microspheres on the hydrochar surface (Figure 2). Thermogravimetric analysis (TGA) showed three mass-loss stages: 2.67% below 190°C (moisture), 18% between 196 - 395°C (hemicellulose/cellulose degradation), and additional loss above 400°C (lignin decomposition) (Figure 3).

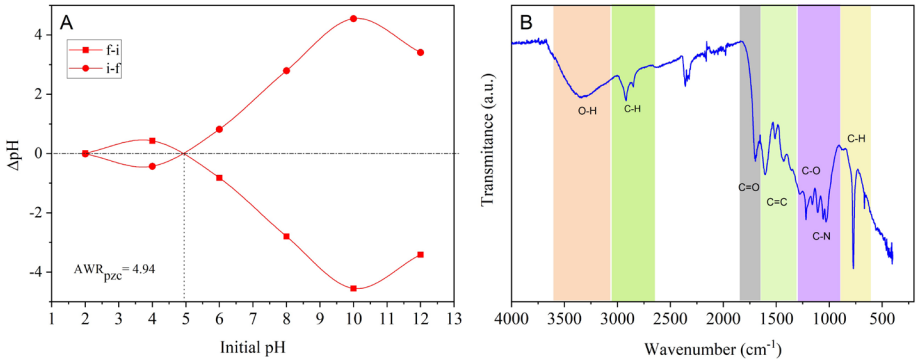

Figure 1. A) Point of zero charges (pH_{pzc}) measured by pH variation experiments for AWR hydrochar, **B)** FTIR spectrum of the AWR hydrochar.

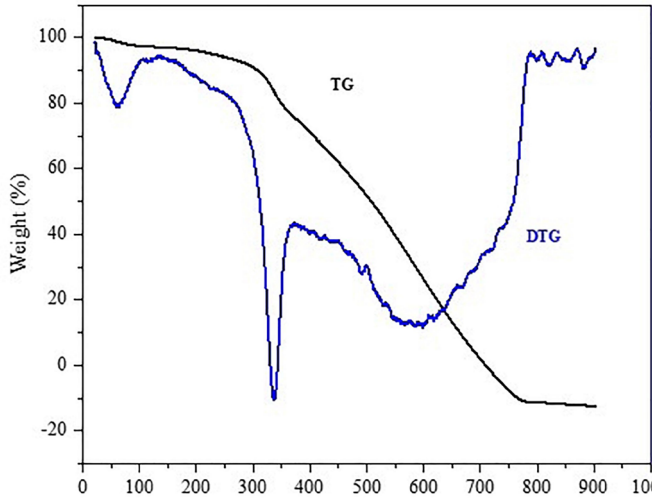

Figure 2. Thermogravimetric analysis (TGA) and derivative thermogravimetry (DTG) of the AWR hydrochar.

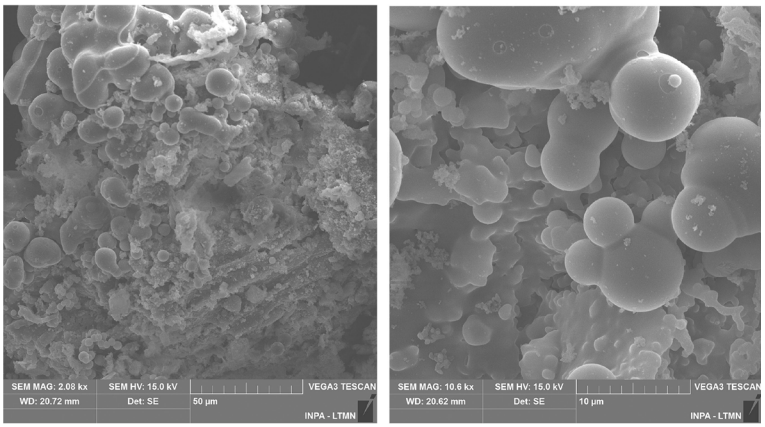

Figure 3. Micrographs of açaí hydrochar (AWR): **A**) 2008 times; and **B**) 10600 times.

Establishing optimal biosorption conditions

The factorial design identified pH 2.0, hydrochar dose 150 mg, and initial Cr (VI) concentration 150 mg L^{-1} as optimal conditions for Cr adsorption, achieving > 99% removal efficiency (Table 3). Statistical analysis indicated that pH had the greatest weight in the data set (-29.60, $p < 0.05$), while interactions between pH and dose (*pHxm*) and pH and concentration (*pHxConc*) were unimportant (Table S1). The Pareto chart (Figure S1) confirmed significance thresholds ($\alpha = 0.05$). The derived model (Equation 3, $R^2 = 0.99$) predicted Cr (VI) removal as

$$\mathbf{R\%} = 69.2156 - 29.6094\,pH - 3.5806m - 1.5894Conc - 4.5281pHm - 9.8356mConc - 10.7831pHmConc \quad (3)$$

Response surface method analysis of second-order interactions supported these ideal conditions to maximize Cr (VI) removal with hydrochar AWR (Figure 4).

Adsorption kinetics

Pseudo-second-order model provided the best fit ($R^2 = 0.99$) for Cr (VI) adsorption, with an equilibrium capacity (Qe) of 25.89 mg g^{-1} and a rate constant (K_2) of 0.00093 (Table 4). Kinetic curves confirmed rapid adsorption within 120 min (Figure 5A-B).

Table 3. Real values of the 2^3 factorial design and experimental results: *m* is the mass of hydrochar (mg) and *Conc* is the concentration of Cr (VI) (ppm).

Tests	Random Order	pH	m(mg)	Conc. (ppm)	Removal (%)
1	1.1	2	50	0.05	99.91
2	6.1	10	50	0.15	54.21
3	8.1	10	150	0.15	7.66
4	2.1	10	50	0.05	33.36
5	7.1	2	150	0.15	99.56
6	5.1	2	50	0.15	99.91
7	3.1	2	150	0.05	96.07
8	4.1	10	150	0.05	66.24
9	8.2	10	150	0.15	9.91
10	3.2	2	150	0.05	95.62
11	1.2	2	50	0.05	99.91
12	6.2	10	50	0.15	54.21
13	4.2	10	150	0.05	66.24
14	2.2	10	50	0.05	25.02
15	7.2	2	150	0.15	99.68
16	5.2	2	50	0.15	99.91

Table 4. Kinetic and isotherm parameters for the adsorption of Cr (VI) on AWR.

Kinetic parameters											
Pseudo-first order				**Pseudo-second order**							
Qe (cal) (mg g^{-1})	23.63			Qe (cal)(mg g^{-1})	25.89						
K_1 (min^{-1})	0.01781			K_2 (g mg^{-1} min^{-1})	0.00093						
R^2	0.93			R^2	0.99						
				Qe(exp)(mg g^{-1})	26.82						
Isotherm Parameters											
Langmuir				**Freundlich**				**Temkin**			
TT (°C)	$Q_{max\ (mg\,g)}$	$K_{L(L/m)}$	R^2	$K_{f(L/g)}$	1/nf	nf	R^2	$AT_{(L\,mg)}$	$B_{(L/g)}$	b_T	R^2
25	17.33	0.65	0.59	8.49	0.2	5.04	0.95	137.93	1.97	1258.2	0.88
35	20.60	0.93	0.94	10.20	0.25	4.06	0.96	15.85	3.63	705.8	0.96
45	22.95	18.84	0.34	20.06	0.15	6.59	0.51	2218.23	2.68	986.9	0.50

Kinetics parameters: solution volume 40 mL, adsorbent mass 0.150 mg and chromium solution concentration of 150mg L^{-1}. Isotherm parameters. Conditions: *pH* = 2, *m* = 0.150 mg and *Conc*. = 150 mg L^{-1}, 120 min.

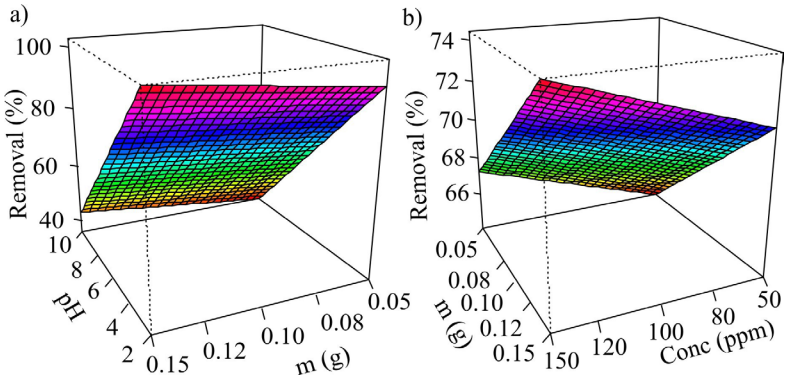

Figure 4. Three-dimensional surface-response plots for the interactive effect of **(A)** mass (m) x pH, and **(B)** Concentration (Conc) x mass (m).

Adsorption isotherm

The Temkin isotherm best describes equilibrium data (R^2 > 0.95), outperforming Langmuir (R^2 = 0.89) and Freundlich (R^2 = 0.91) models (Table 4, Figure 6). The Langmuir maximum monolayer capacity (Q_{max}) 20.60 mg g^{-1}, with an affinity constant (K_L) of 0.93 L.mg^{-1} (Table 4). Isotherm plots and residuals are provided (Figures S2 and S3). AWR's maximum monolayer adsorption capacity at pH 2 (Table 5) exhibits a satisfactory adsorption capacity compared to other adsorbents.

Thermodynamic parameters and adsorption mechanisms

Negative ΔG^0 values (-3623.16 to -11614.41 J mol^{-1}), positive ΔH^0 (115.51 kJ mol^{-1}), and positive ΔS^0 (399.56 J mol^{-1}) indicated spontaneous, endothermic adsorption with increased entropy (Table S2). The van't Hoff plot (Figure S4) confirmed temperature-dependent behavior. The Cr (VI) adsorption mechanisms can include pore filling, surface complexation, electrostatic interaction, and oxidation/reduction (Figure 7).

Table 5. The maximum adsorption capacity (Q_{max}) of AWR compared to the other adsorbents of Cr (VI) adsorption at pH 2.

Adsorbent	Qmax (mg g-1)	References
AWR	**20.60**	This work
Magnetic-modified biochar from raw corncob	25.94	(Hoang *et al.* 2019)
ZnCl2 modified hydrochar	14.0	(Li *et al.* 2020)
AlCl3 modified hydrochar	12.3	(Li *et al.* (2020)
Pristine-modified hydrochar	9.22	(Nguyen *et al.* 2021)
Iron-modified hydrochar	14.33	(Nguyen *et al.* 2021)
Acid-modified poultry litter-derived hydrochar	26.2	(Ghanim *et al.* 2022)
Hydrochar from biomass of *Eupatorium adenophorum* spreng	7.76	(Wang *et al.* 2023c)
Hydrochar derived from coking sludge	19.92	(Zhong *et al.* 2023)

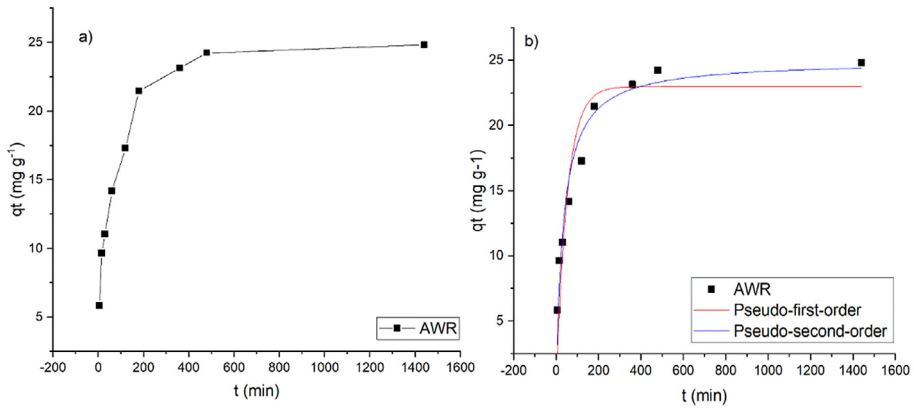

Figure 5. A) Experimental results for adsorption kinetics of Cr (VI) on AWR at 25°C; **B**) adsorption kinetics pseudo-first-order reaction model, and pseudo-second-order reaction fit model for Cr (VI) adsorption on AWR.

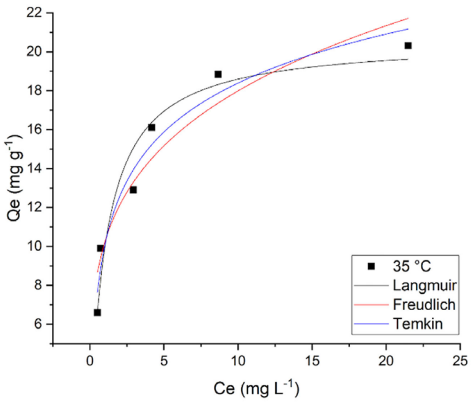

Figure 6. Experimental data of Cr (VI) adsorption on AWR adjusted to isotherm models at 35°C, and Model fit of adsorption isotherm of Cr (VI) adsorption onto AWR with adsorption isotherms (Conditions: *pH* = 2, *m* = 0.150 mg, and *Conc.* = 150 mg L^{-1}, 240 min).

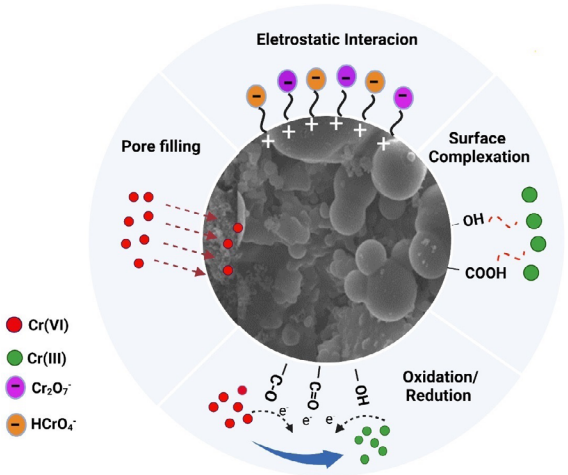

Figure 7. Possible mechanism of Cr (VI) adsorption by AWR.

DISCUSSION

Characteristics of AWR hydrochar

Synthesized hydrochar from açaí seeds (AWR) using the hydrothermal carbonization (HTC) is efficient for Cr (VI) removal. Hydrochar structural and chemical properties and the interaction of oxygenated functional groups contribute to its adsorption effectiveness, while low ash content, high carbon content, and specific surface distinguish it from conventional adsorbents. The oxygenated groups, such as carboxylic and phenolic, derived from the aromatization and polymerization during HTC (Knežević *et al*. 2010), strengthen the interactions between the AWR and Cr (VI). At acidic pH (< pH_{PCZ}), protonation of carboxyl groups (pKa ≅ 5) enhances electrostatic attraction of anionic Cr (VI) species ($HCrO_4^-$ and $Cr_2O_7^{2-}$), while phenolic groups (pKa = 7–10) can mediate the reduction to Cr (III) via electron transfer (Huang *et al*. 2023; Yu *et al*. 2024). Concurrently, basic sites (carbonyl, ether, pyrone, and chromene) contribute π-electron density, potentially stabilizing reduced Cr (III) through complexation (Lobo *et al*. 2024). This dual acid-base functionality allows hydrochar to adsorb anionic and cationic metal species (Shafeeyan *et al*. 2010).

The pH_{PCZ} of 4.94 indicates a protonated surface below this threshold, favoring Cr (VI) anion adsorption (Navas-Cárdenas *et al*. 2023; Hamad *et al*. 2024). At higher pH, deprotonation and OH^- competition diminish removal efficiency, aligning with trends observed in poultry manure and bamboo-derived hydrochars (Ghanim *et al*. 2022; Li *et al*. 2020).

The functional groups identified in this study reflect the complex structure of AWR and provide an understanding of its physical and chemical characteristics. The prominent O–H bending and stretching vibration probably arises from chemically adsorbed water and groups such as alcohols and phenols, a feature consistent with biomass-derived carbonaceous materials (Chen *et al*. 2022; Wu *et al*. 2023; Mutabazi *et al*. 2024). Aliphatic C–H stretching and aromatic C=C vibrations highlight that hydrothermal carbonization can preserve alkyl fragments of the precursor biomass while simultaneously promoting aromatization (Khan *et al*. 2021; Zhang *et al*. 2024), suggesting a carbon matrix rich in π electrons and hydrophobic regions (Zhang *et al*. 2022; Lestari *et al*. 2022). The carbonyl and carboxyl/alkoxy groups suggest a highly oxygenated surface of AWR, which may act as primary ligands for Cr (VI) through ion exchange and electrostatic interaction (Uzun, 2023; Yu *et al*. 2022). The detection of C-N and C-O interactions enhances Lewis basicity and stabilizes adsorbed Cr (VI) through covalent bonding (Escobar *et al*. 2021; Huang *et al*. 2022).

The low H/C and O/C ratios indicate advanced carbonization through dehydration and aromatization during HTC (Wang *et al*. 2022; Ali Babeker *et al*. 2024), improving hydrochar stability and aromaticity (Hejna *et al*. 2023; Guo *et al*. 2025*b*). AWR ash content rises with temperature (Tomczyk *et al*. 2020), but remains lower than typical feedstock (Barros *et al*. 2021), indicating good energy efficiency. High carbon content aligns with its elevated calorific value (Ye *et al*. 2023). In addition, the high C content confirms carbonization through dehydration and deoxygenation, while low H and O content reflect H and O loss as H_2O and CO_2 during HTC (González-Fernández *et al*. 2024; Kousar *et al*. 2024). Low N is advantageous because it avoids nitrogen oxide formation at high temperatures (Shi *et al*. 2023). However, N-containing groups are important in the adsorption (Zhang *et al*. 2022; Chen *et al*. 2023). Furthermore, AWR has a competitive surface area, outperforming oyster mushroom (10 $m^2 g^{-1}$) and corn stalk (5.8 $m^2 g^{-1}$) hydrochars (Romero *et al*. 2025; Lan *et al*. 2024), which highlights the role of specific HTC conditions and unique feedstock characteristics (Netto *et al*. 2022).

The thermal decomposition of AWR is a consequence of the structural components of the biomass. Although the initial mass loss at ~190°C is due to moisture evaporation (Solanki *et al*. 2025), the release of adsorbed water at relatively low temperatures may reflect strong hydrogen bonding between hydroxyl groups and the lignocellulosic matrix, which is a characteristic of biomass hydrophilicity (Zhang *et al*. 2022). Hemicellulose and cellulose degradation ranges (196–395°C), mass loss may be due to dehydration, decarboxylation, and decarbonylation reactions (Mashkoor and Nasar 2020). Above 400°C, additional loss occurs due to lignin degradation (Lobo *et al*. 2024), reinforcing its role as a thermal stabilizer. Furthermore, water extraction during HTC can recover unreacted cellulose, hemicellulose, and lignin from açaí seeds, which can be incorporated into the hydrochar through condensation and polymerization (Dhaouadi *et al*. 2021; Güleç *et al*. 2021).

The formation of carbon microspheres on the surface of AWR may have occurred due to the hydrolysis of cellulose, hemicellulose and lignin fragments in biomass microfibers, in addition to the polymerization and condensation in the soluble phase, increasing the aromatization of the hydrochar (Song *et al*. 2023; Wang *et al*. 2023*a*). The formation of nano to micro-sized carbon spheres on the surfaces of hydrochars is an advantage of the HTC method, which has a wide variety of surface functional groups, such as -OH, -C=O, and -C-OOH (Donar *et al*. 2016). Similar microsphere formation via HTC is reported (Taher *et al*. 2023; Lan *et al*. 2024).

Influence of adsorption parameters

The pH-dependent adsorption of Cr (VI) on AWR illustrates the relationship between the changes in surface charge and the forms of chromium present. Below a pH of 6, Cr (VI) mainly occurs as hydrogen chromate ($HCrO_4^-$) and dichromate ($Cr_2O_7^{2-}$) (Emara *et al*. 2023, Suručić *et al*. 2023). Under these conditions, AWR efficiently removes Cr (VI), due to

the protonation of the surface, attracting the $HCrO_4^-$ and $Cr_2O_7^{2-}$. As nH increases, hydrochar becomes less positive (more negative) and is progressively less attractive to the anionic Cr (VI) (Wu *et al*. 2023). At pH > 6, the amount of OH^- in the solution increases, and $HCrO_4^-$ and $Cr_2O_7^{2-}$ undergo deprotonation to form CrO_4^{2-}. Excessive OH^- in the solution can compete with CrO_4^{2-} for adsorption sites on the AWR surface (Mutabazi *et al*. 2024), thereby reducing the probability of CrO_4^{2-} ions forming bonds with the adsorbent surface (Zhang *et al*. 2022, Mutabazi *et al*. 2024, Zhen *et al*. 2025). Additionally, in alkaline conditions, the redox potential of chromium ions decreases, leading to a reduced transformation from Cr (VI) into Cr (III), which could serve as the electron donor (Bandara *et al*. 2020, Juturu *et al*. 2024). Experimental data indicate reduced removal at higher pH. The effect of initial pH on Cr (VI) removal aligns with previous studies, such as poultry manure hydrochar (Ghanim *et al*. 2022) and modified bamboo sawdust hydrochar (Li *et al*. 2020).

The optimal hydrochar dose (150 mg) reflects a balance between active site availability and particle aggregation. The accentuated increase in sorption capacity is a consequence of higher surface area, more exchangeable sites becoming available for Cr (VI), and the quantity of available functional groups as the adsorbent dose increased (Khalil *et al*. 2021, Mutabazi *et al*. 2024). When the amount of hydrochar is high, biomass particles readily encounter each other, leading to physical interactions, primarily hydrogen bonds, between superficial functional groups (Guo *et al*. 2025*a*). The increase in the initial Cr (VI) concentration led to an increase in the metal removal efficiency. This was attributed to an increased driving force resulting from higher Cr (VI) concentrations (Liu *et al*. 2020, Rind *et al*. 2024).

Kinetic, isotherms, and thermodynamic investigation

The study of adsorption kinetics focuses on the rate at which a solute molecule binds to a solid adsorbent surface (Solanki *et al*. 2025). The pseudo-second-order best described Cr (VI) adsorption onto AWR hydrochar ($R^2 > 0.95$), which indicated that the chemisorption was the rate-limiting step. Thus, the adsorption of Cr (VI) on hydrochar may involve multiple mechanisms such as electrostatic attraction, ion exchange, and surface complexation (Li *et al*. 2020; Ghanim *et al*. 2022; Wang *et al*. 2023*b*; Rohman *et al*. 2024). Similar kinetics have been reported for hydrochar derived from corn straw and corncob for Cd^{2+} and Cr (VI) adsorption (Li *et al*. 2019).

Adsorption isotherms illustrate interaction between an adsorbent and an adsorbate molecule at a constant temperature (Rajendran *et al*. 2022; Nassar *et al*. 2023). The experimental data showed high R^2 values (> 0.95) for both the Temkin and Langmuir isotherm models. However, the Freundlich model had a poor fit (~0.51). The Temkin model describes the multilayer adsorption process where the heat of adsorption decreases linearly with increasing surface coverage (Wang and Guo 2023), and the high binding strength (bT > 8) indicates strong interactions between AWR and Cr (VI) (Choudhary and Paul 2018; Yu *et al*. 2024; Anwar *et al*. 2009). The maximum adsorption capacity (Q_{max}) calculated using the Langmuir model is in close agreement with the testing data, and its adsorption ability is higher than that of other sorbents, suggesting that AWR is an efficient adsorbent. Additionally, an increase in the calculated Q_{max} with an increase in solution temperature suggests that sorption is endothermic (Bilal *et al*. 2022). This may be attributed to the enhanced mobility of the adsorbate ions within the pores of the adsorbent due to a decrease in the viscosity of the solution (Li *et al*. 2010).

Thermodynamic data confirmed the spontaneity and feasibility of Cr (VI) adsorption on AWR ($\Delta G° < 0$) (Emara *et al*. 2023). Furthermore, the adsorption process is endothermic ($\Delta H° > 0$), thus suggesting the predominance of chemical adsorption (Mutabazi *et al*. 2024; Wang *et al*. 2023c). The increased randomness at the hydrochar/solution interface during adsorption ($\Delta S° > 0$) further favors the process (Qu *et al*. 2024).

Possible sorption mechanism and cost analysis of AWR production

Based on the discussions and AWR's complex structure, Cr (VI) adsorption at low pH likely occurs through four mechanisms. Mechanism I involves electrostatic attraction: at low pH, protonation of oxygenated groups imparts positive charges to AWR, attracting anions ($HCrO_4^-$, $Cr_2O_7^{2-}$) (Mei *et al*. 2025). Mechanism II involves Cr (VI) reduction to Cr(III) via electron-donating groups (-OH, C–O, C=O) (Wang *et al*. 2023a). Mechanism III involves surface complexation between Cr(III) and functional groups (Hoang *et al*. 2019). Lastly, pore filling, favored by AWR's high surface area, also contributes to Cr (VI) removal. Thus, AWR adsorption combines physical and chemical interactions.

AWR was produced from abundant açaí seed waste in the Amazon, mitigating environmental harm. The raw material was collected without cost, and transport was ~7.97 USD/ton. Cleaning with deionized water added ~0.06 USD/kg. Producing 1 kg of AWR consumed 0.6 kg of waste and ~3 kWh of electricity (~0.33 USD/kg), with a 30–40% mass loss during HTC. Including 10% for labor and overhead, the total production cost was 9.20 USD/kg, considerably lower than commercial activated carbon (~16.97 USD/kg). Scaling up could further reduce costs. Environmentally, using agro-industrial waste aligns with sustainable waste management and promotes a circular bioeconomy (Yaashikaa *et al*. 2021). However, further studies are needed to comprehensively evaluate economic and environmental impacts.

CONCLUSIONS

The present work highlights the potential of hydrochar derived from açaí biomass as a sustainable and low-cost biosorbent for environmental remediation. The results underscore the relevance of surface oxygenated functional groups and process conditions in enabling effective Cr (VI) adsorption. Beyond confirming the viability of this material, the findings contribute to advancing the understanding of biomass-derived hydrochars in water treatment applications. Future investigations should focus on applying this material to real effluents, exploring adsorption of other pollutants, regeneration and reusability strategies, and optimizing the hydrothermal process through analysis of its liquid-phase by-products. Such efforts can strengthen the role of Amazonian biomass residues in circular economy strategies and sustainable environmental technologies.

ACKNOWLEDGEMENTS

The authors would like to thank *Coordenação de Aperfeiçoamento de Pessoal de Nível Superior* - CAPES/Brazil and *Programa de Pós-graduação em Química* - PPGQ/UFAM for the scholarships to Railane Santos (Ph.D.), to *Conselho Nacional de Desenvolvimento Científico e Tecnológico* - CNPq and Instituto Federal de Educação Ciência e Tecnologia - IFRO for the scholarships to Ana Clara Mendes (graduation student), Naelly Araújo (graduation student) and Nathiely Moraes (high school student), to *Centro de Bionégócios da Amazônia* – CBA for allowing the development of work by some students from the PPGQ-UFAM, to Wyvirlany Lobo, William Pinheiro and Rosangela Duarte for the some caracterization analysis.

REFERENCES

ABNT. 1996. Água - Determinação de cromo hexavalente - Método colorimétrico da difenilcarbazida. *NBR 13738. Água - Determinação de cromo hexavalente - Método colorimétrico da difenilcarbazida*: 5–6.

Ali Babeker, T.M.; Lv, S.; Wu, J.; Zhou, J.; Chen, Q. 2024. Insight into Cu (II) adsorption on pyrochar and hydrochar resultant from Acacia Senegal waste for wastewater decontamination. *Chemosphere* 356: 141881.

Anwar, J.; Shafique, U.; Salman, M.; Waheed-uz-Zaman; Anwar, S.; Anzano, J.M. 2009. Removal of chromium (III) by using coal as adsorbent. *Journal of Hazardous Materials* 171: 797–801.

Arevalo-Gallegos, A.; Ahmad, Z.; Asgher, M.; Parra-Saldivar, R.; Iqbal, H.M.N. 2017. Lignocellulose: A sustainable material to produce value-added products with a zero waste approach—A review. *International Journal of Biological Macromolecules* 99: 308–318.

Bandara, P.C.; Peña-Bahamonde, J.; Rodrigues, D.F. 2020. Redox mechanisms of conversion of Cr (VI) to Cr (III) by graphene oxide-polymer composite. *Scientific Reports* 10: 1–8.

Barros, S. de S.; Oliveira, E. da S.; Pessoa Jr, W.A.G.; Rosas, A.L.G.; de Freitas, A.E.M.; Lira, M.S. de F.; *et al*. 2021. Waste açaí (Euterpe precatoria Mart.) seeds as a new alternative source of cellulose: Extraction and characterization. *Research, Society and Development* 10: 1–16.

Bian, H.; Gao, Y.; Luo, J.; Jiao, L.; Wu, W.; Fang, G.; *et al*. 2019. Lignocellulosic nanofibrils produced using wheat straw and their pulping solid residue: From agricultural waste to cellulose nanomaterials. *Waste Management* 91: 1–8.

Bilal, M.; Ihsanullah, I.; Younas, M.; Ul Hassan Shah, M. 2022. Recent advances in applications of low-cost adsorbents for the removal of heavy metals from water: A critical review. *Separation and Purification Technology* 278: 119510.

Chen, N.; Cui, X.; Sun, X.; Yang, X.; Yang, W.; Ren, N.; *et al*. 2024. Advanced Cr (VI) removal from wastewater using migrating electric field-assisted electrocoagulation combined with capacitive deionization technology. *Journal of Water Process Engineering* 63: 105445.

Chen, X.; Hossain, M.F.; Duan, C.; Lu, J.; Tsang, Y.F.; Islam, M.S.; *et al*. 2022. Isotherm models for adsorption of heavy metals from water - A review. *Chemosphere* 307: 135545.

Chen, Z. Le; Xu, H.; Bai, L.Q.; Feng, Y.L.; Li, B. 2023. Protonated-amino-functionalized bamboo hydrochar for efficient removal of hexavalent chromium and methyl orange. *Progress in Natural Science: Materials International* 33: 501–507.

Choudhary, B.; Paul, D. 2018. Isotherms, kinetics and thermodynamics of hexavalent chromium removal using biochar. *Journal of Environmental Chemical Engineering* 6: 2335–2343.

Dang, H.; Xu, R.; Zhang, J.; Wang, M.; Ye, L.; Jia, G. 2023. Removal of oxygen-containing functional groups during hydrothermal carbonization of biomass: Experimental and DFT study. *Energy* 276: 127436.

Dhaouadi, F.; Sellaoui, L.; Hernández-Hernández, L.E.; Bonilla-Petriciolet, A.; Mendoza-Castillo, D.I.; Reynel-Ávila, H.E.; *et al*. 2021. Preparation of an avocado seed hydrochar and its application as heavy metal adsorbent: Properties and advanced statistical physics modeling. *Chemical Engineering Journal* 419: 129472.

Donar, Y.O.; Çağlar, E.; Sinağ, A. 2016. Preparation and characterization of agricultural waste biomass based hydrochars. *Fuel* 183: 366–372.

Elhassan, M.; Kooh, M.R.R.; Chou Chau, Y.F.; Abdullah, R. 2024. Hydrochar from Shorea spp.: a dual-purpose approach for sustainable biofuel and efficient methylene blue adsorbent. *Biomass Conversion and Biorefinery* 15: 5779–5793.

Emara, M.M.; Hafez, S.T.; Khalil, T.E.; Kashyout, A.E.H.B.; El-Dissouky, A.; El-Sayed, D.S. 2023. Electronic and structural perturbations of microporous ZIF-67 nanoparticles and Cr (VI) molecule during adsorptive water decontamination unveiled by experimental and quantum computational investigations. *Journal of Molecular Liquids* 390: 123042.

Escobar, O.D.S.; Azevedo, C.F.; Swarowsky, A.; Adebayo, M.A.; Netto, M.S.; Machado, F.M. 2021. Utilization of different parts of Moringa oleifera Lam. seeds as biosorbents to remove Acid Blue 9 synthetic dye. *Journal of Environmental Chemical Engineering* 9: 105553.

Fang, J.; Zhan, L.; Ok, Y.S.; Gao, B. 2018. Minireview of potential applications of hydrochar derived from hydrothermal carbonization of biomass. *Journal of Industrial and Engineering Chemistry* 57: 15–21.

de Freitas, F.A.; de Sá Barros, S.; Saron, C.; Lobo, W. V.; dos Santos, R.I.L.; Las-Casas, B.; *et al*. 2024. Lignocellulose Characterization And Exploitation. *Reference Module in Earth Systems and Environmental Sciences*: 1–12.

Ghanim, B.; Leahy, J.J.; O'Dwyer, T.F.; Kwapinski, W.; Pembroke, J.T.; Murnane, J.G. 2022. Removal of hexavalent chromium (Cr (VI)) from aqueous solution using acid-modified poultry litter-derived hydrochar: adsorption, regeneration and reuse. *Journal of Chemical Technology and Biotechnology* 97: 55–66.

González-Fernández, L.A.; Medellín-Castillo, N.A.; Navarro-Frómeta, A.E.; Castillo-Ramos, V.; Sánchez-Polo, M.; Carrasco-Marín, F. 2024. Optimization of hydrochar synthesis conditions for enhanced Cd(II) and Pb(II) adsorption in mono and multimetallic systems. *Environmental Research* 261: 119651.

Güleç, F.; Riesco, L.M.G.; Williams, O.; Kostas, E.T.; Samson, A.; Lester, E. 2021. Hydrothermal conversion of different lignocellulosic biomass feedstocks – Effect of the process conditions on hydrochar structures. *Fuel* 302: 121166.

Guo, T.; Bulin, C.; Li, C.; Xin, G.; Bao, J.; Song, J. 2025a. Experimental and statistical physics illumination of Pb(II) adsorption on magnetic chitosan-graphene oxide surface. *Separation and Purification Technology* 354: 128867.

Guo, W.; Zhang, Z.; Feng, Y.; Zhang, Y. 2024. Unravelling heterogenous adsorption performance of hydrochar particle and key properties in heavy metal immobilization relative to corresponding residual bulk hydrochar. *Process Safety and Environmental Protection* 192: 1073–1084.

Guo, W.; Zhang, Z.; Wang, B.; Xue, L.; Feng, Y. 2025b. Novel insights into released hydrochar particle derived from typical high nitrogen waste biomass: Special properties, microstructure and formation mechanism. *Waste Management* 193: 517–528.

Habib, S.S.; Naz, S.; Fazio, F.; Cravana, C.; Ullah, M.; Rind, K.H.; *et al*. 2024. Assessment and Bioaccumulation of Heavy Metals in Water, Fish (wild and Farmed) and Associated Human Health Risk. *Biological Trace Element Research* 202: 725–735.

Hamad, N.; Galhoum, A.A.; Saad, A.; Wageh, S. 2024. Efficient adsorption of cationic and anionic dyes using hydrochar nanoparticles prepared from orange peel. *Journal of Molecular Liquids* 409: 125349.

Hejna, M.; Świechowski, K.; Białowiec, A. 2023. Study on the Effect of Hydrothermal Carbonization Parameters on Fuel Properties of Sewage Sludge Hydrochar. *Materials* 16: 6903.

Hoang, L.P.; Van, H.T.; Nguyen, L.H.; Mac, D.H.; Vu, T.T.; Ha, L.T.; *et al*. 2019. Removal of Cr (VI) from aqueous solution using magnetic modified biochar derived from raw corncob. *New Journal of Chemistry* 43: 18663–18672.

Huang, C.; Yu, C.; Wang, G.; Zhang, J.; Ning, X.; Wang, C. 2022. Comparison of structural characteristics and combustibility analysis about hydrochar and pyrochar. *Journal of Thermal Analysis and Calorimetry* 147: 10509–10523.

Huang, S.A.; Teng, H.J.; Su, Y.T.; Liu, X.M.; Li, B. 2023. Trithiocyanurate-functionalized hydrochar for effectively removing methylene blue and Pb (II) cationic pollutants. *Environmental Pollution* 337: 122585.

Irshad, M.A.; Sattar, S.; Nawaz, R.; Al-Hussain, S.A.; Rizwan, M.; Bukhari, A.; *et al*. 2023. Enhancing chromium removal and recovery from industrial wastewater using sustainable and efficient nanomaterial: A review. *Ecotoxicology and Environmental Safety* 263: 115231.

Juturu, R.; Selvaraj, R.; Murty, V.R. 2024. Efficient removal of hexavalent chromium from wastewater using a novel magnetic biochar composite adsorbent. *Journal of Water Process Engineering* 66: 105908.

Kambo, H.S.; Dutta, A. 2015. A comparative review of biochar and hydrochar in terms of production, physico-chemical properties and applications. *Renewable and Sustainable Energy Reviews* 45: 359–378.

Katsas, K.; Diamantis, D. V.; Linos, A.; Psaltopoulou, T.; Triantafyllou, K. 2024. The impact of exposure to hexavalent chromium on the incidence and mortality of oral and gastrointestinal cancers and benign diseases: a systematic review of observational studies, reviews and meta-analyses. *Environments - MDPI* 11: 11.

Khalil, U.; Shakoor, M.B.; Ali, S.; Ahmad, S.R.; Rizwan, M.; Alsahli, A.A.; *et al*. 2021. Selective removal of hexavalent chromium from wastewater investigation. *Water* 13: 12.

Khan, N.; Mohan, S.; Dinesha, P. 2021. Regimes of hydrochar yield from hydrothermal degradation of various lignocellulosic biomass: A review. *Journal of Cleaner Production* 288: 125629.

Knežević, D.; Van Swaaij, W.; Kersten, S. 2010. Hydrothermal conversion of biomass. II. conversion of wood, pyrolysis oil, and glucose in hot compressed water. *Industrial and Engineering Chemistry Research* 49: 104–112.

Koc, I.; Cobanoglu, H.; Canturk, U.; Key, K.; Kulac, S.; Sevik, H. 2024. Change of Cr concentration from past to present in areas with elevated air pollution. *International Journal of Environmental Science and Technology* 21: 2059–2070.

Kousar, S.; Fan, M.; Javed, K.; Rashid, M.; Zhang, S.; Hu, X. 2024. Hydrothermal carbonization of fruit peels of varied origin forms hydrochar of distinct capability for adsorption of methylene blue. *Journal of Water Process Engineering* 65: 105799.

Lan, Y.; Luo, Y.; Yu, S.; Ye, H.; Zhang, Y.; Xue, M.; *et al*. 2024. Cornstalk hydrochar produced by phosphoric acid-assisted hydrothermal carbonization for effective adsorption and photodegradation of norfloxacin. *Separation and Purification Technology* 330: 125543.

Lestari, D.I.; Yuliansyah, A.T.; Budiman, A. 2022. Adsorption studies of KOH-modified hydrochar derived from sugarcane bagasse for dye removal: Kinetic, isotherm, and thermodynamic study. *Communications in Science and Technology* 7: 15–22.

Li, F.; Zimmerman, A.R.; Hu, X.; Gao, B. 2020. Removal of aqueous Cr (VI) by Zn- and Al-modified hydrochar. *Chemosphere* 260: 127610.

Li, X.; Yu, Y.; He, R.; Zhen, Q.; She, D. 2025. Mechanistic insights into cadmium removal from environmental waters using silicon-enhanced lignin-derived hydrochar and pyrochar. *Separation and Purification Technology* 355: 129727.

Li, Y.; Tsend, N.; Li, T.K.; Liu, H.; Yang, R.; Gai, X.; *et al*. 2019. Microwave assisted hydrothermal preparation of rice straw hydrochars for adsorption of organics and heavy metals. *Bioresource Technology* 273: 136–143.

Li, Y.; Hagos, F.M.; Chen, R.; Qian, H.; Mo, C.; Di, J.; *et al*. 2021. Rice husk hydrochars from metal chloride-assisted hydrothermal carbonization as biosorbents of organics from aqueous solution. *Bioresources and Bioprocessing* 8: 99.

Liu, N.; Zhang, Y.; Xu, C.; Liu, P.; Lv, J.; Liu, Y.Y.; *et al*. 2020. Removal mechanisms of aqueous Cr (VI) using apple wood biochar: a spectroscopic study. *Journal of Hazardous Materials* 384: 121371.

Li, Y.; Du, Q.; Wang, X.; Zhanga, P.; Wang, D.; Wang, Z.; *et al*. 2010. Removal of lead from aqueous solution by activated carbon prepared from Enteromorpha prolifera by zinc chloride activation. *Journal of Hazardous Materials* 183: 583–589.

Liu, N.; Zhao, J.; Du, J.; Hou, C.; Zhou, X.; Chen, J.; *et al*. 2024. Non-phytoremediation and phytoremediation technologies of integrated remediation for water and soil heavy metal pollution: A comprehensive review. *Science of the Total Environment* 948: 174237.

Lobo, W.V.; Loureiro Paes, O.A. da R.; Pinheiro, W.; Soares, E.R.; de Souza, M.P.; dos Santos Sousa, A.; *et al*. 2024. Application of chemically modified waste tucumã (Astrocaryum aculeatum) seeds in the biosorption of methylene blue: kinetic and thermodynamic parameters. *Environmental Science and Pollution Research*. 31: 34097-34111.

Magdziarz, A.; Wilk, M.; Wądrzyk, M. 2020. Pyrolysis of hydrochar derived from biomass – Experimental investigation. *Fuel* 267: 117246.

Malool, M.E.; Moraveji, M.K. 2025. A comprehensive synergistic study of process parameters on co-hydrothermal carbonization of digested sewage sludge and sugarcane bagasse: hydrochar yield, lead adsorption capacity, and physicochemical properties. *Journal of Water Process Engineering* 69: 106692.

Maniscalco, M.P.; Volpe, M.; Messineo, A. 2020. Hydrothermal carbonization as a valuable tool for energy and environmental applications: A review. *Energies* 13.

Mashkoor, F.; Nasar, A. 2020. Magsorbents: Potential candidates in wastewater treatment technology – A review on the removal of methylene blue dye. *Journal of Magnetism and Magnetic Materials* 500: 166408.

Mei, Y.; Zhuang, S.; Wang, J. 2025. Adsorption of heavy metals by biochar in aqueous solution: A review. *Science of the Total Environment* 968: 178898.

Melo, P.S.; Selani, M.M.; Gonçalves, R.H.; Paulino, J. de O.; Massarioli, A.P.; Alencar, S.M. de. 2021. Industrial Crops & Products Açaí seeds : An unexplored agro-industrial residue as a potential source of lipids, fibers, and antioxidant phenolic compounds. *Industrial Crops & Products* 161: 113204.

Mutabazi, E.; Qiu, X.; Song, Y.; Li, C.; Jia, X.; Hakizimana, I.; *et al*. 2024. Cr (VI) adsorption on activated carbon, sludge derived biochar, and peanut shells derived biochar: Performance, mechanisms during the reuse process, and site energy distribution analysis. *Journal of Water Process Engineering* 57: 104679.

Nassar, A.E.; El-Aswar, E.I.; Rizk, S.A.; Gaber, S.E.S.; Jahin, H.S. 2023. Microwave-assisted hydrothermal preparation of magnetic hydrochar for the removal of organophosphorus insecticides from aqueous solutions. *Separation and Purification Technology* 306: 122569.

Navas-Cárdenas, C.; Caetano, M.; Endara, D.; Jiménez, R.; Lozada, A.B.; Manangón, L.E.; *et al*. 2023. The role of oxygenated functional groups on cadmium removal using pyrochar and hydrochar derived from *Guadua angustifolia* residues. *Water* 15: 525.

Netto, M.S.; Georgin, J.; Franco, D.S.P.; Mallmann, E.S.; Foletto, E.L.; Godinho, M.; *et al*. 2022. Effective adsorptive removal of atrazine herbicide in river waters by a novel hydrochar derived from Prunus serrulata bark. *Environmental Science and Pollution Research* 29: 3672–3685.

Nguyen, L.H.; Van, H.T.; Chu, T.H.H.; Nguyen, T.H.V.; Nguyen, T.D.; Hoang, L.P.; *et al*. 2021. Paper waste sludge-derived hydrochar modified by iron (III) chloride for enhancement of ammonium adsorption: An adsorption mechanism study. *Environmental Technology and Innovation* 21: 101223.

Nie, D.; Ma, R.; Zhang, Y.; Wang, W.; Nie, G.; Liu, G.; *et al*. 2024. Efficient removal of Cr (VI) from wastewater by composite adsorptive membrane modified with polyethyleneimine (PEI). *Separation and Purification Technology* 346: 127410.

Nur-E-Alam, M.; Mia, M.A.S.; Ahmad, F.; Rahman, M.M. 2020. An overview of chromium removal techniques from tannery effluent. *Applied Water Science* 10: 1–22.

Qu, J.; Shi, S.; Li, Y.; Liu, R.; Hu, Q.; Zhang, Y.; *et al*. 2024. Fe/N co-doped magnetic porous hydrochar for chromium(VI) removal in water: Adsorption performance and mechanism investigation. *Bioresource Technology* 394: 1–10.

Rajendran, S.; Priya, A.K.; Senthil Kumar, P.; Hoang, T.K.A.; Sekar, K.; Chong, K.Y.; *et al*. 2022. A critical and recent developments on adsorption technique for removal of heavy metals from wastewater - A review. *Chemosphere* 303: 135146.

Rind, I.K.; Memon, N.; Sarı, A.; Khuhawar, M.Y.; Tuzen, M.; Naveed ul Hasan, S.; *et al*. 2024. Magnetic nanoparticles loaded hydrochar for effective Cr (VI) removal from water: Batch and column studies. *Materials Chemistry and Physics* 318: 129077.

Rohman, G.A.N.; Aziz, M.A.; Nawaz, A.; Elgzoly, M.A.; Hossain, M.M.; Razzak, S.A. 2024. High-performance biochar from Chlorella pyrenoidosa algal biomass for heavy metals removal in wastewater. *Separation and Purification Technology* 341: 126870.

Romero, E.; Méndez, A.; Moral-Rodríguez, A.I.; Gascó, G.; Nogales, R. 2025. Comparative efficiency of hydrochar and biochar from spent Pleurotus ostreatus substrate for removing ciprofloxacin from water. *Journal of Water Process Engineering* 69.

Sato, M.K.; de Lima, H.V.; Costa, A.N.; Rodrigues, S.; Pedroso, A.J.S.; de Freitas Maia, C.M.B. 2019. Biochar from Acai agroindustry waste: Study of pyrolysis conditions. *Waste Management* 96: 158–167.

Shafeeyan, M.S.; Daud, W.M.A.W.; Houshmand, A.; Shamiri, A. 2010. A review on surface modification of activated carbon for carbon dioxide adsorption. *Journal of Analytical and Applied Pyrolysis* 89: 143–151.

Shi, Y.; Li, C.; Chai, R.; Wu, J.; Wang, Y. 2023. Effect of different hydrothermal parameters on calorific value and pyrolysis characteristics of hydrochar of kitchen waste. *Energies* 16.

Solanki, A.; Ahamad, Z.; Gupta, V. 2025. Upcycling waste biomass: Alkali-modified watermelon rind as a lignocellulosic bioadsorbent for copper ion removal. *Industrial Crops and Products* 224: 120340.

Song, H.; Zhou, J.; He, S.; Ma, Q.; Peng, L.; Yin, M.; *et al*. 2023. Efficient removal of heavy metals from contaminated sunflower straw by an acid-assisted hydrothermal process. *International Journal of Environmental Research and Public Health* 20: 1311.

Suručić, L.; Janjić, G.; Marković, B.; Tadić, T.; Vuković, Z.; Nastasović, A.; *et al*. 2023. Speciation of hexavalent chromium in aqueous solutions using a magnetic silica-coated amino-modified glycidyl methacrylate polymer nanocomposite. *Materials* 16: 2233.

Taher, T.; Maulana, S.; Mawaddah, N.; Munandar, A.; Rianjanu, A.; Lesbani, A. 2023. Low-temperature hydrothermal carbonization of activated carbon microsphere derived from microcrystalline cellulose as carbon dioxide (CO_2) adsorbent. *Materials Today Sustainability* 23: 100464.

Tan, M.; Yang, S.; Song, C.; He, Z.; Wang, J.; Liu, Y.; *et al*. 2024. Selective removal of chromium and chloride by flow electrode capacitive deionization (FCDI) with carrier-facilitated ion exchange membrane. *Chemical Engineering Journal* 499: 156182.

Tee, G.T.; Gok, X.Y.; Yong, W.F. 2022. Adsorption of pollutants in wastewater via biosorbents, nanoparticles and magnetic biosorbents: A review. *Environmental Research* 212: 113248.

Thakur, H. 2024. Hydrochar Production Methods: Comparative Insights into Hydrothermal and Microwave Processes. *African Journal of Biological Sciences* 6: 3033–3044.

Tomczyk, A.; Sokołowska, Z.; Boguta, P. 2020. Biochar physicochemical properties: pyrolysis temperature and feedstock kind effects. *Reviews in Environmental Science and Biotechnology* 19: 191–215.

Tounsadi, H.; Khnifira, M.; Khalidi, A.; Abdennouri, M.; Barka, N. 2025. Effective removal of heavy metals from aqueous solutions using activated biomass: Analytical interpretation via molecular dynamic simulation, mathematical and statistical approaches. *Journal of Molecular Structure* 1319: 139371.

Țurcanu, A.A.; Matei, E.; Râpă, M.; Predescu, A.M.; Coman, G.; Predescu, C. 2022. Biowaste valorization using hydrothermal carbonization for potential wastewater treatment applications. *Water* 14: 2344.

Uzun, Z.Y. 2023. Investigation of fuel properties of hydrochars obtained from pomegranate peel: characterization and combustion kinetic. *Biomass Conversion and Biorefinery https://doi.org/10.1007/s13399-023-03840-7*.

Wang, J.; Guo, X. 2023. Adsorption kinetics and isotherm models of heavy metals by various adsorbents: An overview. *Critical Reviews in Environmental Science and Technology* 53: 1837–1865.

Wang, J.; Wang, Y.; Wang, J.; Du, G.; Khan, K.Y.; Song, Y.; *et al*. 2022. Comparison of cadmium adsorption by hydrochar and pyrochar derived from Napier grass. *Chemosphere* 308: 136389.

Wang, X.; Zhao, Y.; Deng, J.; Zhou, Y.; Yuan, S. 2023a. Study on the influence mechanism of mineral components in biochar on the adsorption of Cr (VI). *Fuel* 340: 127631.

Wang, Y.; Xu, Y.; Lu, X.; Liu, K.; Li, F.; Wang, B.; *et al*. 2023b. Biomass-based hydrothermal carbons for the contaminants removal of wastewater: a mini-review. *International Journal of Molecular Sciences* 24.

Wang, Z.; Lu, N.; Cao, X.; Li, Q.; Gong, S.; Lu, P.; *et al*. 2023c. Interactions between Cr (VI) and the hydrochar: The electron transfer routes, adsorption mechanisms, and the accelerating effects of wood vinegar. *Science of the Total Environment* 863: 160957.

Wibowo, Y.G.; Taher, T.; Khairurrijal, K.; Ramadan, B.S.; Safitri, H.; Sudibyo, S.; *et al*. 2024. Recent advances in the adsorptive removal of heavy metals from acid mine drainage by conventional and novel materials: A review. *Bioresource Technology Reports* 25: 101797.

Wu, Z.; Chen, Z.; Tang, J.; Zhou, Z.; Chen, L.; Fang, Y.; *et al*. 2023. Efficient adsorption and reduction of Cr (VI) in water using one-step H3PO4-assisted prepared *Leersia hexandra* Swartz hydrochar. *Materials Today Sustainability* 21: 100260.

Yaashikaa, P.R.; Kumar, P.S.; Saravanan, A.; Vo, D.V.N. 2021. Advances in biosorbents for removal of environmental pollutants: A review on pretreatment, removal mechanism and future outlook. *Journal of Hazardous Materials* 420: 126596.

Yadav, S.; Priyadarshini, M.; Asce, S.M.; Ahmad, A.; Asce, M.; Ghangrekar, M.M.; *et al*. 2025. Hydrochar Nanocatalyst for Emerging Pollutant Remediation, Sustainable Development, and Circular Economy. 29: 1–18.

Yang, X.; Xiong, J.; Cao, L.; Zhang, Y.; Wu, P.; Shi, Y.; *et al*. 2025. One-step electrochemical reduction and precipitation removal of Cr (VI) in acid wastewaters using amidoxime-functionalized carbon felt. *Desalination* 593: 118257.

Ye, L.; Zhang, J.; Wang, G.; Wang, C.; Mao, X.; Ning, X.; *et al*. 2023. Feasibility analysis of plastic and biomass hydrochar for blast furnace injection. *Energy* 263: 125903.

Yu, K.; Huan, W.W.; Teng, H.J.; Guo, J.Z.; Li, B. 2024. Effect of oxygen-containing functional group contents on sorption of lead ions by acrylate-functionalized hydrochar. *Environmental Pollution* 349: 123921.

Yu, S.; Yang, X.; Zhao, P.; Li, Q.; Zhou, H.; Zhang, Y. 2022. From biomass to hydrochar: Evolution on elemental composition, morphology, and chemical structure. *Journal of the Energy Institute* 101: 194–200.

Zhang, X.; Chen, F.; Liu, S.; Lou, J.; Liu, W.; Rousseau, D.P.L.; *et al*. 2024. Synthesis, characterization, and methylene blue adsorption isotherms of hydrochars derived from forestry waste and agro-residues. *Biomass Conversion and Biorefinery* 14: 1809–1824.

Zhang, Y.; Zhang, T. 2022. Biowaste Valorization to Produce Advanced Carbon Material-Hydrochar for Potential Application of Cr (VI) and Cd (II) Adsorption in Wastewater: A Review. *Water* 14: 3675.

Zhang, Y.N.; Guo, J.Z.; Wu, C.; Huan, W.W.; Chen, L.; Li, B. 2022. Enhanced removal of Cr (VI) by cation functionalized bamboo hydrochar. *Bioresource Technology* 347: 126703.

Zhen, H.G.; Hu, C.; Yang, L.; Du Laing, G. 2025. Hydrochar produced from mixed feedstocks as efficient adsorbent for selenium and chromium removal from acidic wastewater. *Desalination* 593: 118152.

Zhong, J.; Zhu, W.; Wang, X.; Sun, J.; Mu, B.; Xu, Y.; *et al*. 2023. Effect mechanism of iron conversion on adsorption performance of hydrochar derived from coking sludge. *Science of the Total Environment* 898: 165427.

Zulfiqar, U.; Haider, F.U.; Ahmad, M.; Hussain, S.; Maqsood, M.F.; Ishfaq, M.; *et al*. 2023. Chromium toxicity, speciation, and remediation strategies in soil-plant interface: A critical review. *Frontiers in Plant Science* 13: 1–33.

RECEIVED: 26/09/2024
ACCEPTED: 02/05/2025
ASSOCIATE EDITOR: André Willerding
DATA AVAILABILITY: The datasets used or analyzed during the current study are available from the corresponding author on reasonable request.

SUPPLEMENTARY MATERIAL

Santos *et al.* Removal of Cr (VI) from synthetic effluents using hydrochar from waste açaí (*Euterpe precatoria* Mart.) seeds as low-cost biosorbent

ADSORPTION KINETICS EQUATIONS

Pseudo-first order (PFO) adsorption:

$$q_t = q_e(1 - e^{k_1 t}) \qquad (S1)$$

Pseudo-second order (PSO):

$$q_t = \frac{k_2 q_e^2 t}{1 + k_2 q_e t} \qquad (S2)$$

where:

qt and *qe* are the amounts of Cr (VI) adsorbed in the specific time (*t),* and when the equilibrium is achieved (mg g^{-1}), respectively, K_1 is the rate constant of the pseudo-first-order adsorption process (1 min^{-1}), and K_2 is the rate constant of adsorption (g mg^{-1} min^{-1}) of the pseudo-second-order model.

ISOTHERMAL MATHEMATICAL EQUATIONS

Langmuir model:

$$Q_e = \frac{Q_{max} * K_L C_e}{1 + Q_{max} * K_L C_e} \qquad (S3)$$

Freundlich model:

$$Q_e = K_F * C_e^{\frac{1}{n}} \qquad (S4)$$

Temkin model:

$$Q_e = \frac{RT}{b_T}\ ln\ ln\ A_T * C_e \qquad (S5)$$

where:

Ce = equilibrium concentration of the Cr VI (mg L^{-1}), Qe = amount of Cr (VI) adsorbed at equilibrium per unit weight of AWR (mg g^{-1}), Qmax = maximum monolayer coverage capacity (mg g^{-1}), K_L = Langmuir isotherm constant (L mg^{-1}) related to the binding energy of adsorption, and R_L = dimensionless separation factor indicating the nature and favorability of adsorption process. K_F = Freundlich indicator of adsorption capacity, and 1/nF = Intensity of adsorption, indicating surface heterogeneity and the favorability of the adsorption process. b_T = the Temkin isotherm constant related to the heat of adsorption and A_T = the Temkin isotherm equilibrium binding constant (L g^{-1}), R = universal gas constant (8.314 J mol^{-1} K^{-1}), T = absolute temperature in Kelvin, and B = RT/b_T = constant related to heat of sorption (J mol^{-1}) obtained either from intercept or slope.

THERMODYNAMIC PARAMETERS

Gibbs free energy (ΔG°)

$$K_e = \frac{C_{Ads}}{C_e} \qquad (S6)$$

$$ln_{ke} = \frac{\Delta S^0}{R} - \frac{\Delta H^0}{RT} \qquad (S7)$$

Gibbs free energy (ΔG°)

$$\Delta G^0 = \Delta H° - T\Delta S° \qquad (S8)$$

enthalpy (ΔH°)

and entropy (ΔS°)

where:

Ke is the equilibrium constant, CAds is the amount of adsorbent (mg g^{-1}), Ce is the equilibrium concentration of the dye in the solution (mg L^{-1}), R is the universal gas constant (8.314 J mol^{-1} K^{-1}), and T is the temperature (K). ΔH° (J mol^{-1}) and ΔS° (J mol^{-1} K^{-1}) were calculated from the slope and intercept of the plot ln_{Ke} vs 1/t.

ANOVA FACTORIAL DESIGN

Table S1. Effects for Cr (VI) removal efficiency by adsorption on AWR.

	Effects	Standard Error	*t*	p-value
Constant[a]	69.2156	0.5406	128.024	1.55e-14
pH	-29.6094	0.5406	-54.767	1.37e-11
m	-3.5806	0.5406	-6.623	0.000165
Conc.	-1.5894	0.5406	-2.940	0.018716
pH x m	-4.5281	0.5406	-8.375	3.13e-05
pH x Conc.	-0.5044	0.5406	-0.933	0.378163b
m x Conc.	-9.8356	0.5406	-18.192	8.57e-08
pH x m x Conc.	-10.7831	0.5406	-19.945	4.16e-08

[a] m = mass of hydrochar (mg), Conc. = concentration of Cr (VI) (ppm), and [b] = p > 0,05.

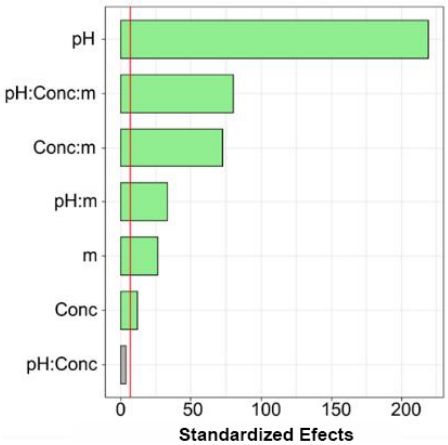

Figure S1. Pareto diagram for Cr (VI) removal efficiency by adsorption on AWR. Where: m is the mass of hydrochar (mg), and Conc is the concentration of Cr (VI) (mg.L^{-1}).

ISOTHERMS

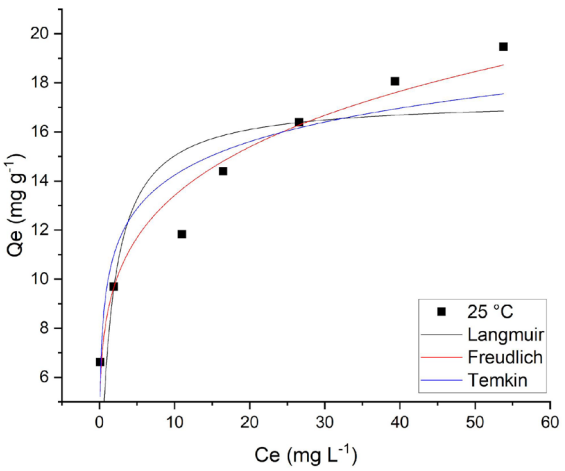

Figure S2. Model fit of adsorption isotherm of Cr VI adsorption onto AWR at 25 °C. (Conditions: *pH* = 2, *m* = 0.150 mg, and *Conc.* = 150 mg L^{-1}, 240 min).

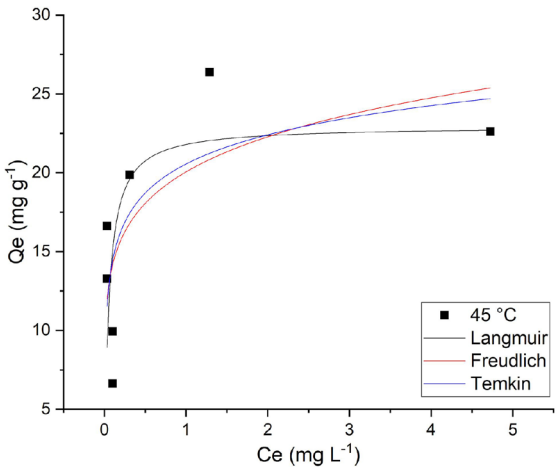

Figure S3. Model fit of adsorption isotherm of Cr VI adsorption onto AWR at 45 °C. (Conditions: *pH* = 2, *m* = 0.150 mg, and *Conc.* = 150 mg L^{-1}, 240 min).

THERMODYNAMIC PARAMETERS

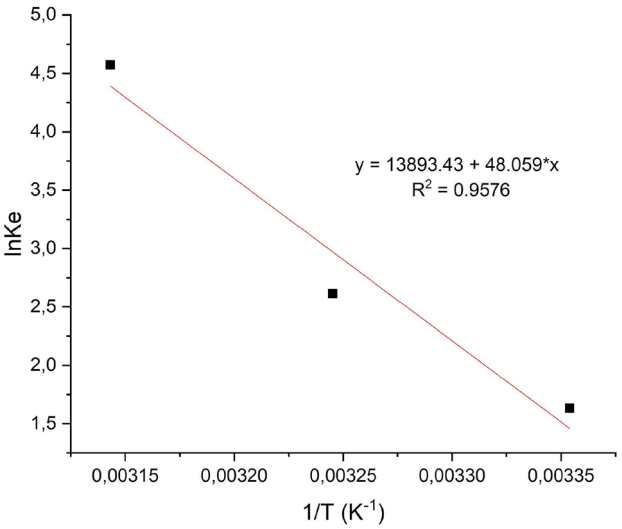

Figure S4. Van't Hoff plot for adsorption of Cr VI on AWR. (Conditions: *pH* = 2, *m* = 0.150 mg, and *Conc.* = 150 mg L^{-1}, 240 min

Table S2. Thermodynamic parameters for the adsorption of Cr (VI) ions onto AWR.

Temp. (K)	ΔG⁰ (J mol-1)	ΔH⁰ (kJ mol-1)	ΔS⁰ (J mol-1)	R²
298.15	-3623.165	115.506402	399.562526	0.9576
308.15	-7618.790			
318.15	-11614.416			